Analysis of the relationship between vegetation indices and forage nutritional parameters in Mediterranean semi-arid rainfed grasslands

Toro-Mujica P [a,*] , Lozano-Parra J [b], Enríquez-Hidalgo D [c,d,e]

[a] Institute of Agri-Food, Animal and Environmental Sciences (ICA3), Universidad de O'Higgins, San Fernando, 3070000, Chile
[b] Department of Art and Territorial Sciences, Universidad de Extremadura, Cáceres, 10071, Spain
[c] Bristol Veterinary School, University of Bristol, Langford, BS40 5DU, United Kingdom
[d] Rothamsted Research, Sustainable Agriculture Sciences, North Wyke, Okehampton, Devon, EX20 2SB, United Kingdom
[e] Faculty of Agronomy and Forestry Engineering, Department of Animal Science, Pontifical Catholic University of Chile, Santiago, Chile

ABSTRACT

Information about herbage availability and its nutritional value is fundamental to implementing efficient and precise grassland management. However, obtaining such information is time-consuming and expensive, representing an important burden particularly when the herbage resources are scarce. The use of new technologies, such as remote sensing, has been proposed as a promising alternative. The objectives of this study were 1) to characterize the seasonal variation of herbage biomass and nutritional value of the naturalized grassland of the Mediterranean semi-arid zone, and 2) to develop regression models to predict the nutritional value of naturalized grasslands using vegetational indices (VIs) as predictive variables. The herbage growth and nutritional value of the grasslands were monitored. At the same time, multispectral images were captured, and VIs were generated. Results showed differences in botanical composition and nutritional values among sampling sites. The VIs that presented the best adequacy, based on values of R^2 and RMSE, for determining dry matter, crude protein, neutral, and acid detergent fibers were NDVI, CLRG, CLRG and GNDVI, respectively. The quick estimation of the nutritional value of grasslands from VIs obtained through aerial images offers significant potential for improving planning processes.

1. Introduction

Efficient and precise grassland management and feed planning in extensive livestock farms require accurate information about herbage availability (Serrano et al., 2016). This information is crucial for determining sustainable livestock numbers based on herbage-carrying capacity (Barnetson et al., 2020) and for avoiding grassland and soil degradation caused by over- or under-grazing (Tang et al., 2019). In Central Chile, a large portion of the livestock production systems in the Mediterranean semi-arid zone relies on grasslands for feeding. However, during the summer there is a characteristic forage deficit that requires a tunned balance between the natural supply of fodder, its administration, and the need for supplementary feed. Unfortunately, the available information regarding the nutritional value and its temporal evolution is outdated, spanning several decades (Ruiz, 1996). Furthermore, climate change, by delaying the onset of the rainy season, has postponed the start of grasslands' growing period, which results in a shorter growing season (Liu et al., 2019), rendering the available information no longer representative. In this context, the use of aerial images to determine the availability and quality parameters of naturalized grasslands emerges as a viable and dynamic alternative with the potential for implementation in the Mediterranean semi-arid zone in Central Chile. However, there are challenges associated with obtaining estimation models, including the rapid seasonal changes in the phenological state of annual pastoral species, spatial location, the damage caused by wildfires, the variability and seasonal fluctuation of pastoral species present in the natural grassland, and the heterogeneous state of soil conservation (Liu et al., 2019; Castillo et al., 2020; Espinoza et al., 2020). The last two aspects are of particular concern resulting from decades of intensive specialized monoculture crop production (mainly wheat) and historical mismanagement of grazing (both over and under-grazing) (Espinoza et al., 2020).

Numerous techniques and instruments have been used to estimate herbage availability. Among the traditional techniques, the most

---

common and oldest method is the manual collection of herbage biomass along defined transects using quadrat harvests or estimations (Barnetson et al., 2020). This technique requires many samples of known areas to estimate grassland productivity. The plate meter and electronic capacitance probe are commonly used instruments to estimate herbage availability, both of which necessitate the establishment of transects and multiple measurements (Serrano et al., 2016; Barnetson et al., 2020). As pastoral resources become scarce, the precision of estimates needs to increase, and planning around herbage availability is not enough; therefore, the need arises for nutritional assessments of resources to meet the nutrient requirements of grazing livestock. Molle et al. (2008) describe the variation in the nutritive value of Mediterranean pastures and its impact on the nutrition of dairy sheep, primarily driven by the imbalance between crude protein and energy. These variations necessitate management interventions, including optimizing pasture fertilization and incorporating supplements. Similarly, Fenetahun et al. (2021) emphasize the importance of assessing forage nutritional value to adjust pasture rotation, develop adaptive strategies that ensure year-round feed availability for livestock, and formulate balanced diets more efficiently, thereby reducing dependence on costly supplements.

Proximal and Van Soest fiber analyses are standard methods used to estimate the nutritional value of pastures and forages (Van Soest et al., 1991). Although these analyses are accurate, they are slow and expensive. Near-infrared reflectance spectroscopy (NIRS) technology has overcome these limitations with faster and more affordable analyses (Park et al., 1998; Thomson et al., 2018; Oliveira et al., 2020). However, the use of NIRS analysis requires a long calibration process and the use of uncommon feedstuffs can lead to misinterpretations. Moreover, both traditional analyses and NIRS, require the collection of numerous samples in the field and subsequent processing, demanding significant labor and cost.

With advancements in technology, new methods for monitoring *in situ* availability and nutritional value of grass and forages have emerged, some of which are based on obtaining vegetation indices (VIs) using remote sensing images. VIs are derived by mathematically combining various spectral bands obtained from images taken with multispectral cameras. These cameras can be portable or installed in unmanned aerial vehicles (UAVs) and satellites (Paltsyn et al., 2017). VIs obtained from multispectral images have been investigated for more than three decades. However, the emergence of UAVs and easier access to satellite images has increased their use. For instance, VIs have been related to quantitative variables such as the height, availability, or covered area of arboreal and non-arboreal plant species (e.g., Fern et al., 2018; Lussem et al., 2018; Lussem et al., 2019; Dube et al., 2021). Spectral VIs represent unique signatures of green vegetation, and different types of vegetation often exhibit distinctive variability due to different parameters such as the shape and size of plants, water content, associated background, and phenological stage (Fajji et al., 2017). The assessment of relationships between forage nutritional parameters and wavelengths or VIs is more recent (Posada-Asprilla et al., 2019; Barnetson et al., 2020). Forage nutritional parameters such as neutral detergent fiber (NDF), crude protein (CP), nitrogen (N), Carbon:Nitrogen ratio (C:N) have already been linked to wavelengths or VIs (Beeri et al., 2007). The use of UAVs to capture multispectral images for estimating VIs has been a focus of research in the past decade (Poley and McDermid, 2020). Wachendorf et al. (2018) point out that UAVs and hyperspectral imaging systems may play a major role in the rapid and non-destructive sampling of temperate grasslands' properties and in improving agricultural use of grasslands.

Thereby, considering changes in precipitation and temperature patterns, the lack of updated information on the nutritional value of rainfed natural grasslands in Central Chile (Alignier et al., 2021), and the emergence of new technologies for rapid determination of forage nutritional value, this study aimed to address the following question: How effective are VIs in predicting the forage nutritional parameters of natural grasslands in Mediterranean semi-arid zones to support on-farm decision-making? To answer this question, the research focused on two main objectives: (1) to characterize the seasonal variation in the nutritional value of naturalized grasslands in the Mediterranean semi-arid zone, and (2) to develop regression models to predict the nutritional value of naturalized grasslands using vegetation indices (VIs) as predictive variables.

2. Materials and methods

2.1. Study area

The study was carried out in the O'Higgins Region, part of Central Chile, located between 33°00′ S and 35° 01′ S and between 70° 02′ W and the Pacific Ocean. Specifically, the study focused on the dryland areas of the communities of La Estrella (S1), Marchigüe (S2) and Pumanque (S3) (Fig. 1).

The prevailing climate in the study areas is a temperate Mediterranean semi-arid climate with annual mean temperature values around 13.3 °C. Over the past decades, an increasing temperature trend has been observed. As shown in Fig. 2, the mean temperature has consistently exceeded the long-term average by more than 0.45 °C over the last two decades.

The annual precipitation is irregular, with June and July as the wettest months, with a historical average between 100 and 300 mm per month (Pizarro, 2007). Long-term annual average rainfall (1901–2021) ranges between 602 mm in northern study areas and 729 mm in the southern one although in the last decades, the annual precipitation has been decreasing (Harris et al., 2020). The most common Mediterranean semi-arid pastoral zone is characterized by a steppe where *Vachellia caven* dominates the arboretum strata and the main species observed (and its percentage presence) in the naturalized grasslands are *Avena barbata, Vulpia dertonensis and Bromus mollis (between 11-65%), Lolium multiflorum (2–65%), Briza minor (25–40%), Medicago polymorpha* (0–22%), *Hordeum leporinum, Aira caryophyllea, Trifolium glomeratum, Trifolium striatum and Trifolium arvense* (Ruiz, 1996).

As described by Allen et al. (2011), a naturalized grassland consists of species primarily introduced from other geographical regions that have become established and persisted under the prevailing environmental and management conditions over an extended period. These grasslands are typically utilized by cattle or sheep under continuous grazing or rotational grazing systems, often with a limited number of paddocks.

The soils in the O'Higgins Region are mainly classified as Luvisols and, secondly, as Calcisols, according to the Harmonized World Soil Database (HWSD) (FAO, 2012). Generally, the texture of the topsoil can be considered sandy clay loam, while at deeper depths, as clay loam. The study areas show the properties summarized in Appendix A.

A study area was selected in each of three communities (La Estrella (S1), Marchigüe (S2), and Pumanque (S3), Fig. 1). Sheep flock management is common in this region, with stocking rates ranging from 0.2 to 0.6 livestock units (LU) per hectare (Toro-Mujica and García, 2025; Ruiz, 1996).

Multispectral images were captured and sampling was conducted at the three sites. The linear distances between S1 and S2 were 14.14 km, between S2 and S3 were 29.5 km, and between S1 and S3 were 29.4 km. Each site had three 10 × 10 m exclusion plots located at varying distances of 65–170 m from each other. The fence height was approximately 1.5 m constructed with 4-inch idlers, sheep mesh, and barbed wire (Appendix B). Each exclusion plot was considered a replication to explore site variability and reduce bias. The localization of the plots within each site is shown in Fig. 1. The geographic coordinates of each exclusion plot are detailed in Appendix C.

Meteorological stations (Decagon Weather Station model EM50G) (Appendix B) were installed at two of the study sites (S1 and S3) to relate the beginning of the growing season with the meteorological conditions. Meteorological data included temperature, precipitation, relative
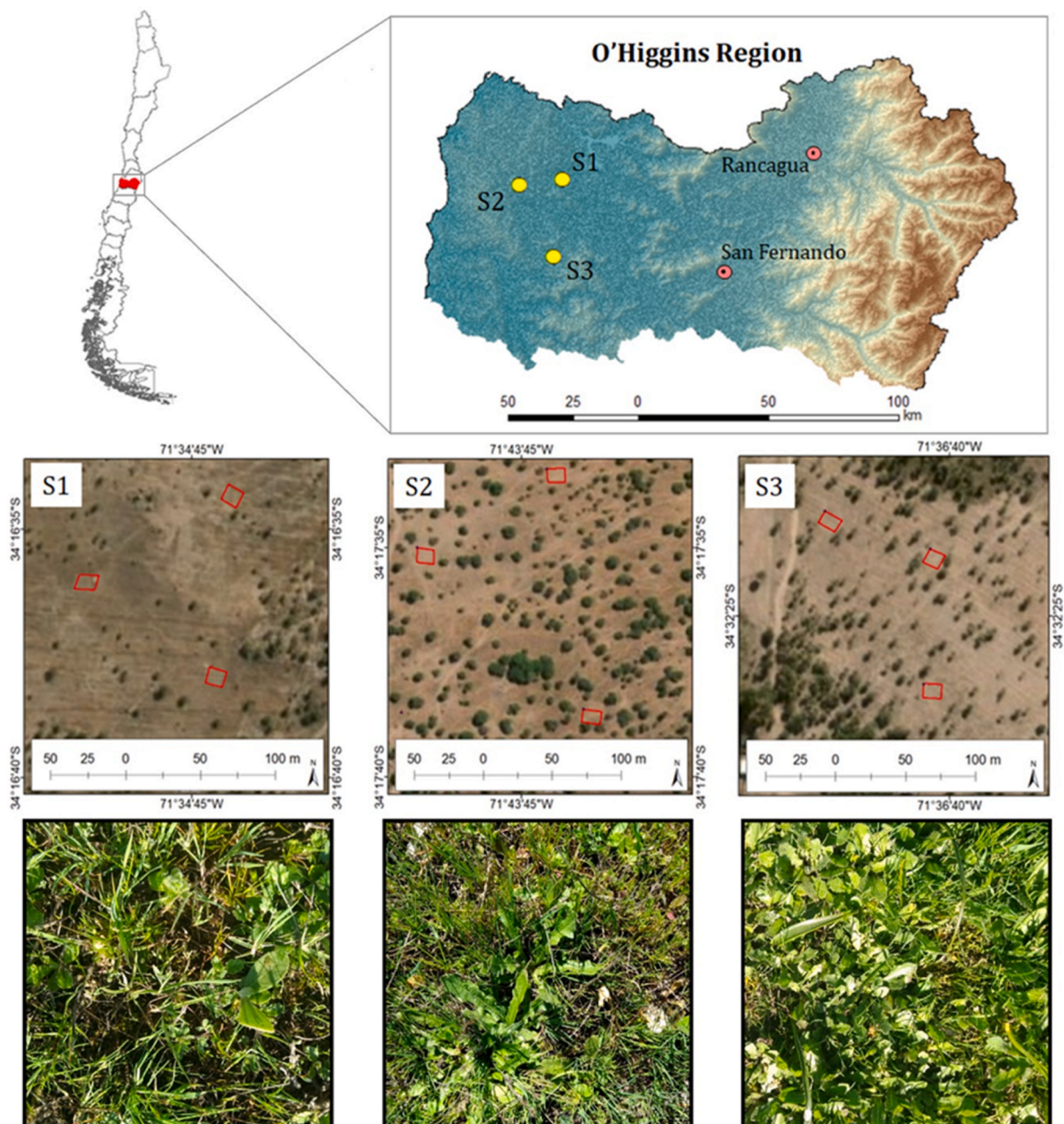
Fig. 1. Location of the study sites in the O'Higgins Region. S1, S2, S3 = Sampling area 1, 2 and 3, respectively and grass growth in sites 1, 2, and 3.

humidity, wind speed and direction, and soil temperature and moisture (at a depth of 20 cm) recorded every hour.

2.2. Grass sampling

Grass samples were obtained twice a month from August to December 2018 at each site and each exclusion plot when the compressed herbage height exceeded 3 cm. For the estimation of compressed herbage height a Jenquip® forage plate meter (NZ Agriworks Ltd, Feilding, New Zealand) was used following a similar protocol as for Enriquez-Hidalgo et al. (2016). At least ten herbage heights were taken by following an imaginary W shape within each exclusion plot. Measurements were taken at a distance of at least 0.5 m away from the plot fences to minimize edge confounding effects. Electric hand shears (Makita UM603DWY) were used to clip vegetation at a height of 3 cm above ground level. Three randomly placed subsamples of 0.5 × 0.5 m per exclusion plot were used. The sample consisted of all standing herbaceous vegetative material available in an area of 0.75 m² (0.5 m × 0.5 m x 3 squares). The samples were collected into paper bags and taken to the food and feed analysis laboratory of the Pontificia Universidad Católica de Chile for further processing. The samples were weighed and then oven-dried at 60 °C for 48 h to determine dry matter concentration (DM) and used to estimate DM biomass per hectare. Dry samples were milled (1 mm), placed in sealed plastic bags, and stored at room temperature in a low-humidity cabinet for chemical analysis, including crude protein (CP), neutral detergent fiber (NDF), and acid detergent fiber (ADF) concentrations. AOAC (2005) methods were used to estimate DM (method 2001.12) and CP (nitrogen concentration x 6.25; method 2001.11) concentrations. The NDF and ADF were determined using the Van Soest et al. (1991) method.

2.2.1. Botanical composition characterization

The botanical composition of the experimental sites was determined in November 2018 using an adaptation of the Ecological Outcome
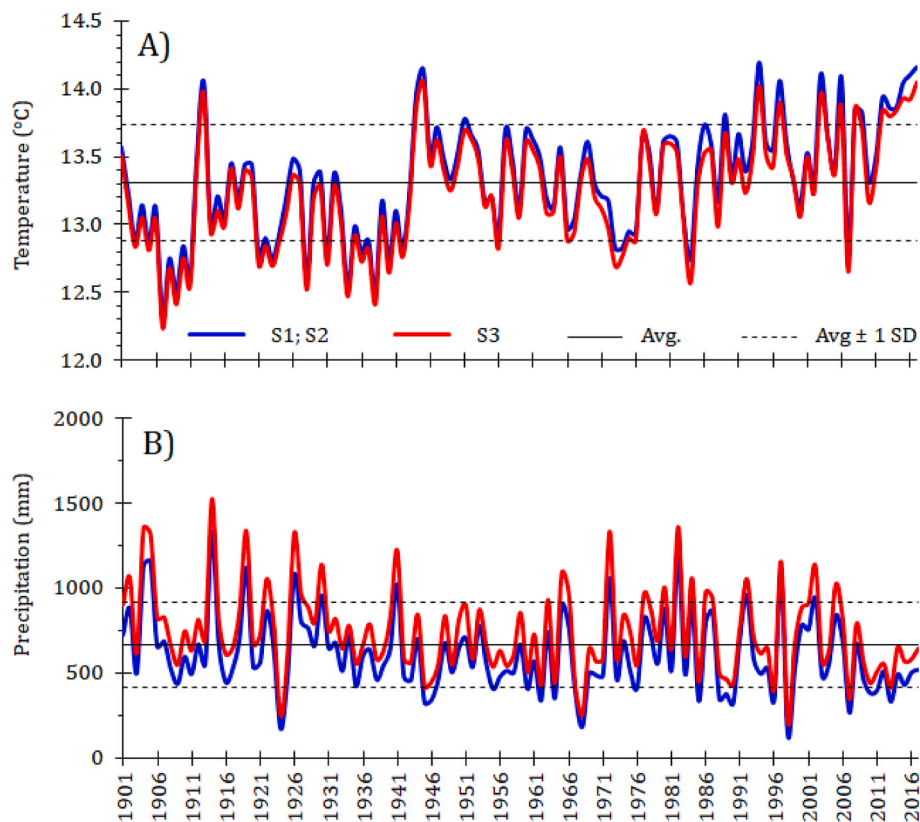
Fig. 2. Mean annual temperature (A) and annual precipitation in the study areas from 1901 to 2016. S1, S2, S3 = Sampling area 1, 2 and 3, respectively. Avg and SD = Average and Standard Deviation, respectively, obtained by monthly data (1901–2016) from Harris et al. (2020).

Verification (EOV) program (Savory Institute, 2018). Briefly, two 10 m transects were marked within each exclusion plot from each experimental site. Every plant species encountered every 25 cm along the transect (400 points for each transect) was identified and then the percentage of individuals encountered was calculated.

2.2.2. Capturing of multispectral imaging

Multispectral images were captured with a single DJI INSPIRE 2 UAV equipped with Parrot Sequoia® multispectral camera (Parrot, Paris, France) and a sunshine sensor. The Parrot Sequoia® camera had four single-band cameras in the green (550 nm ± 40 nm), red (660 nm ± 40 nm), red-edge (735 nm ± 10 nm), and near-infrared (NIR) (790 nm ± 40 nm) bands. The sunshine sensor measured the incoming radiation. Pix4D capture software (Pix4D, San Francisco, CA, USA) was used for flight planning and capturing aerial images. The UAV data were collected during the grassland growing season (June–December 2018) twice a month immediately before the herbage measurements were taken. All images were taken between 12:00 and 14:00 in clear or semi-clear sky conditions. The flight altitude above the ground level was 100 m, the front overlap and side were 80%, and the image ground sample distance was 9.42 cm/px.

2.2.3. Image processing and obtaining VIs

Agisoft Photoscan Professional (Agisoft LLC, St. Petersburg, Russia) was used to preprocess the multispectral images for alignment and reflectance calibration. The information from the sunshine sensor was used for reflectance calibration. Complete orthogonal rasters were made with each band for the three sites.

Subsequently, the following eight VIs were calculated using the QGis software (QGIS, QGIS Development Team, 2022): simple ratio vegetation index (RVI), normalized difference vegetation index (NDVI), green chlorophyll index (GCI), red edge normalized difference vegetation

index (RNDVI), red edge chlorophyll index (CLRG), soil-adjusted vegetation index (SAVI) and plant senescence reflectance index (PSRI) (Appendix D). The selection of indices was based on their ability to detect changes in the physiological state, color (consequence of pigment content), coverage, and biomass availability (Villoslada Peciña et al., 2021). Additionally, the selection considered the availability of spectral bands and the results of previous studies on the capacity of these indices to estimate the nutritional composition of grasslands. The selected indices combine the red, red-edge, near-infrared, and green bands. The red band indicates the chlorophyll concentration; the near-infrared band is strongly associated with the leaf cellular structures, being sensitive to green vegetation (Bannari et al., 1995). Combining these two bands through the RVI, NDVI, and SAVI indices allows to differentiate vegetation from soils. It determines photosynthetically active biomass related to the quantity, quality, and development of vegetation cover and its vigor (Dusseux et al., 2022). By incorporating a constant of soil, SAVI reduces the influence of light and dark soil on the index, which is suitable for semi-arid areas such as the study area (Vani and Mandla, 2017; Munyati, 2022). The red-edge band has been used to estimate the chlorophyll content (Gitelson et al., 2003a, 2005; Clevers and Gitelson, 2013) and foliar nitrogen (Ramoelo et al., 2012). Both RNDVI and CLRG use the red-edge band, incorporating themselves in searching for CP estimation models. PSRI is sensitive to the ratio of chlorophylls (Chl) to carotenoids (Car) content and, therefore, a good indicator of the maturation processes of plants (Zhou et al., 2019); which considering the shortening of the vegetative phase of the species in the grassland under study deserves to be evaluated. The GCI and GNDVI indices, when incorporating the green band, help monitor the physiological state of the plants and their relationship with climatic variables. GCI and GNDVI are more sensitive to chlorophyll variation in the crop than NDVI. This made their use more appropriate in crops with dense canopies or in more advanced stages of development than NDVI (Mangewa et al., 2022). On

the other hand, as Asrar et al. (1984) pointed out, the VIs have shown better sensitivity than individual spectral bands for detecting biomass and their nutritional compositions. For the calculation of each index, one hundred measurement points were randomly selected within the area corresponding to each exclusion plot (Fig. 3b). The measurement points were taken at a distance of at least 0.5 m away from the plot fences to minimize the edge confounding effects. For each point, the eight vegetation indices were obtained (Fig. 3c), and then, an average per plot was obtained.

2.3. Statistical analysis

2.3.1. Data processing

Monthly averages were calculated for the variables under study: Herbage biomass (Ton DM/ha), Dry matter (%), CP (%), NDF (%), and ADF (%) to characterize the change of the nutritional value and herbage biomass of the naturalized grassland throughout the growing season.

The eight VIs indices were matched with the respective nutritional value (DM, CP, NDF, and ADF). These data were then stored in a database along with information on acquisition frequency (twice a month), study site, and plot details.

Firstly, the normal distribution of each variable data was tested. The outliers (more than 1.5 times the interquartile range above the third quartile or below the first quartile) were identified using box plot graphics for their subsequent elimination. Then, the homoscedasticity of the variances was evaluated. As there were fewer than 50 samples for each variable, the Shapiro Wilks analysis was used to check for normality. The Levene test was used to evaluate the homoscedasticity of the variances, utilizing the mean or median as the centrality statistic depending on the normality of the data. The ANOVA test was used for the variables with normal distribution while the Kruskal-Wallis test was used for the remaining variables. Multiple comparisons of means analysis were conducted with the DMS test to compare between months.

Data for each variable were used according to the following statistical model:

$$Y_{ijk} = \mu + \alpha_j + \beta_k + (\alpha\beta)_{jk} + \varepsilon_{ijk}$$

Where Y_{ijk}: Dependent variable; μ: Overall mean; α_j: Effect of month; β_k: Effect of community, $(\alpha\beta)_{jk}$: Interaction month/study site; ε_{ijk}: Experimental error; j: 7–12, k:1–3, i:1-3.

2.4. Development and verification of estimation models

Initially, the relationships between each independent variable (Vegetation index, VI) and the dependent variable were graphed to preview the existing functional relationships, such as linear, exponential, or logarithmic. The two most apparent functional relationships were selected to further develop regression models. The regression models were developed under the internal validation method called "Data-splitting". The total samples were divided into two groups: one group containing 75% of the samples used for model development, and the other group containing 25% of the samples used to assess the model's performance (Picard and Berk, 1990). Afterward, the fit statistics for each parameter and VI were compared. The statistics included the coefficient of determination (R^2), root mean square error (RMSE), mean absolute error (MAE), and relative root mean square error (rRMSE) (Ren and Zhou, 2014; Gao et al., 2019; Xu et al., 2021). Statistical analysis was performed using R programming language version March 1, 1073 (R Core Team, 2021), the car (Fox and Weisberg, 2019), carData (Fox et al., 2020), caret (Kuhn, 2021), and tidyverse (Wickham et al., 2019) packages.

3. Results

3.1. Weather data

The average temperature and precipitation patterns recorded in the year of study (2018) for the two weather stations are presented in Fig. 4.

The weather patterns across the two weather stations were similar in terms of the average temperatures but differed in the distribution of precipitation. The notable distinction was the occurrence of delayed rainfall events recorded at the Pumanque weather station that contributed more than 10 mm to the accumulated precipitation.

3.2. Grass sampling

During June, the stored soil moisture allowed the beginning of germination; however, the low temperatures prevented to maintain the growth of the seedlings until September. The compressed herbage height increased notably from September until November, going from 2 to 5 cm (Fig. 5).

Subsequently, the compressed herbage height began to decrease due to senescence but this decrease was not significant. Due to the low precipitation observed during the autumn months (March–April) and the low temperatures in the winter months (May–July), the naturalized pasture only reached the compressed herbage height cutting target (>3 cm) in October (Fig. 5). Consequently, values for the variables of herbage biomass and nutritional value were only obtainable for October, November and December. Nonetheless, in some of the exclusion plots, the cutting height was not even reached during the first or second visit in
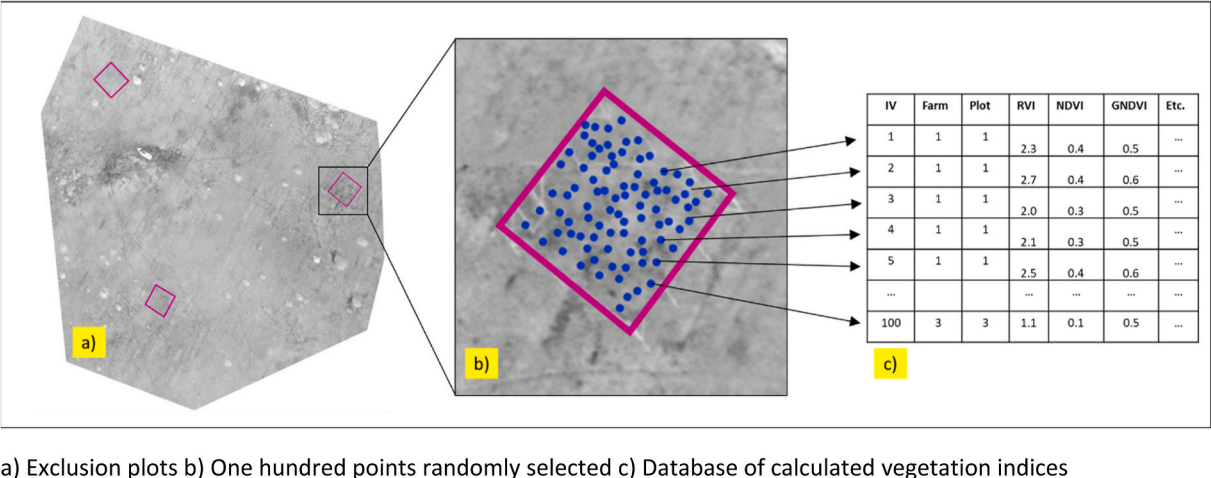

a) Exclusion plots b) One hundred points randomly selected c) Database of calculated vegetation indices

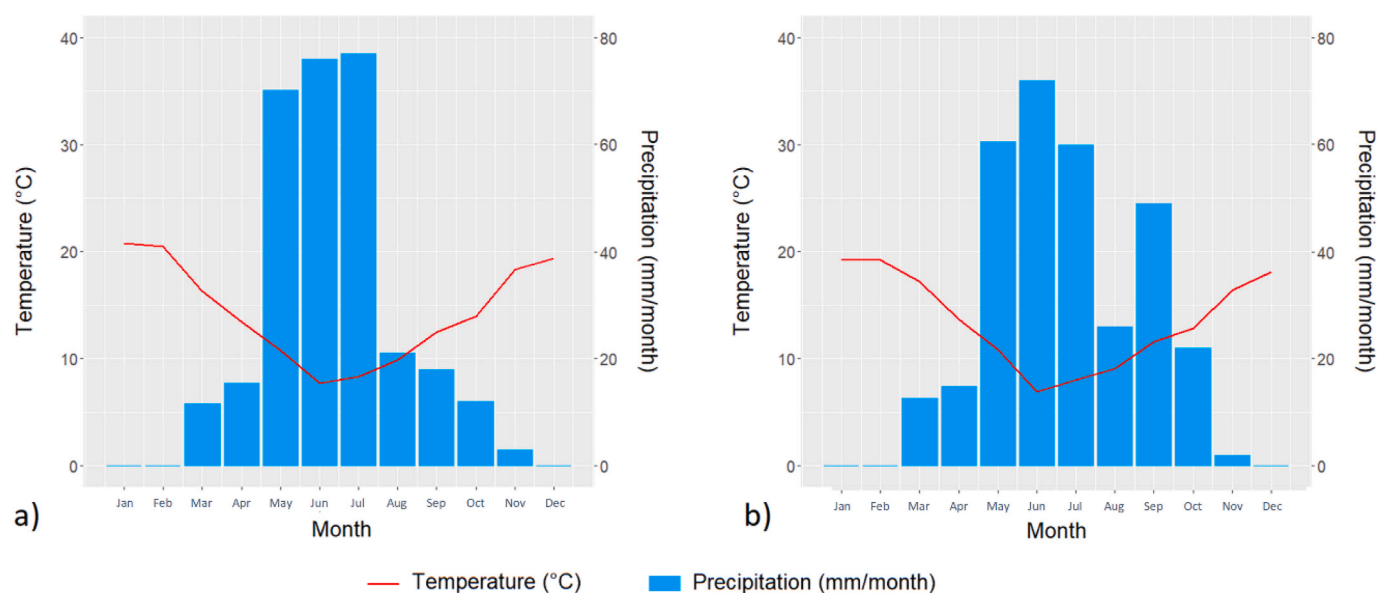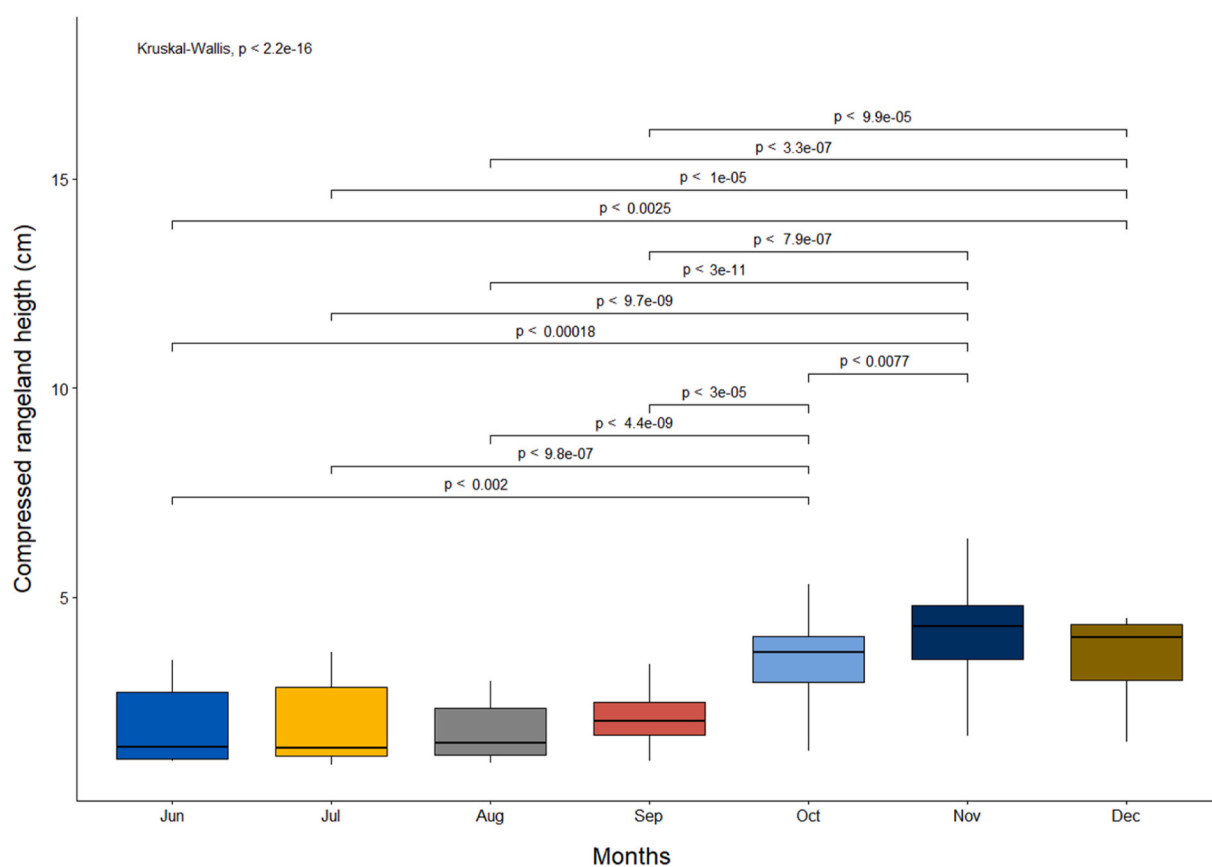**Fig. 3.** Stages for obtaining vegetation indices.

Fig. 4. Weather patterns at two study sites a) Site 1: La Estrella (Annual precipitation: 304.2 mm) and b) Site 3: Pumanque (Annual precipitation: 319 mm) in 2018.

Horizontal lines indicate significant differences between indicated months.

Fig. 5. Kruskal-Wallis's test and multiple comparison of means for compressed height in the months of study.

October, resulting in a total of only 39 samples.

3.3. Seasonal variation in forage nutritional and botanical composition

The average values of the nutritional parameters evaluated are presented in Table 1.

The herbage biomass reached an average maximum of 1.16 Ton DM/ha, showing an increase of more than 40% between October and December, reflecting the highest growth rate of 11.7 kg DM/ha/day observed in October. Seasonal rates of change in DM, CP, NDF and ADF

Table 1
Monthly evolution of herbage biomass and nutritional composition variables of the naturalized pasture during the 2018 growing season across three sites (Mean ± SD).

Variable	October 2nd and 19th (n = 15)	November 5th and 19th (n = 16)	December 12th (n = 8)	p value
Herbage biomass (Ton DM/ha)	0.67 ± 0.33[a]	1.05 ± 0.55[b]	1.16 ± 0.50[c]	0.031
DM (%)	28.75 ± 8.59[a]	66.45 ± 23.95[b]	95.99 ± 0.73[c]	<0.001
CP (%)	14.63 ± 3.99[a]	8.22 ± 1.18[b]	5.85 ± 1.9[b]	<0.001
NDF (%)	50.09 ± 10.17	55.73 ± 6.14	55.59 ± 4.68	0.105
ADF (%)	25.22 ± 4.77[a]	31.0 ± 2.88[b]	33.69 ± 1.46[b]	<0.001

*Within row, averages with different superscript differ significantly (p < 0.05).

performed as expected. The maximum DM was 96%, with an accelerated change from 28.8 to 96% between October and December, which reveals the shortening of the growing season. The maximum value of crude protein was 14.6% during October. NDF was similar between the three months and ADF did not show significant differences between November and December, when reached its maximum value (32.4%). No outliers were detected for herbage biomass, NDF, and ADF. However, DM had one outlier in December, and CP had two outliers in November, which were subsequently excluded from the dataset analysis.

The study site at Marchigüe (S2) was mainly dominated by *Hordeum murinum* (29.9%) and *Briza minor* (6.9%), while *Leontodon saxatilis* (23.5 and 21.1%, respectively) and *Briza minor* (14.9 and 20.8%, respectively) were the dominant species for the study sites of La Estrella (S1) and Pumanque (S3). The following species were identified with a minor participation (<6%) in all the study sites: *Lolium multiflorum (5.4%), Chenopodium album (4.1%), Cynosurus cristatus (3.9%), Avena fatua (3.2%), Bellardia trixago(3%), Hypochaeris radicata (2.2%), Trifolium aureum (1.9%), Cirsium arvense (1.5%), Bromus hordeaceus (1.2%), Chamaemelum nobile (1.1%)* and *Erodium cicutarium (1.1%)* and *Pasithea coerulea (0.8%)*.

3.4. Model construction and performance evaluation

The first stage in model construction was image capturing, which could be carried out from June to December; however, due to the lack of nutritional value data from the pasture, only the images obtained from October to December were finally considered. The monthly average values of the eight VIs are shown in Table 2. In all VIs the values obtained in October differed significantly from the other two months evaluated.

The computed VIs displayed different functional forms and trends as

Table 2
Monthly means and descriptive statistics of the vegetation indices evaluated (Mean ± SD) (N = 1800 points).

Vegetation indexes	October	November	December	p value
RVI	5.31 ± 3.57[a]	1.17 ± 0.11[b]	1.06 ± 0.08[b]	<0.001
NDVI	0.57 ± 0.2[a]	0.1 ± 0.08[b]	0.03 ± 0.04[b]	<0.001
GNDVI	0.65 ± 0.09[a]	0.49 ± 0.03[b]	0.47 ± 0.04[b]	<0.001
GCI	4.18 ± 1.6[a]*	1.98 ± 0.26[b]	1.84 ± 0.29[b]	<0.001
RNDVI	0.03 ± 0.03[a]	0.01 ± 0.01[b]	0.01 ± 0.02[b]	<0.001
CLRG	0.07 ± 0.06[a]	0.01 ± 0.02[b]	0.02 ± 0.04[b]	<0.001
SAVI	0.85 ± 0.3[a]	0.14 ± 0.11[b]	0.04 ± 0.06[b]	<0.001
PSRI	0.09 ± 0.1[a]	0.49 ± 0.1[b]	0.59 ± 0.04[b]	<0.001

RVI = ratio vegetation index, NDVI = normalized difference vegetation index, GNDVI = green normalized difference vegetation index, GCI = green chlorophyll index, RNDVI = red normalized difference vegetation index, CLRG = red edge chlorophyll index, SAVI = soil-adjusted vegetation index, PSRI = plant senescence reflectance index.
*Within row, averages with different superscript differ significantly (p < 0.05).

pasture maturation advanced (Fig. 6). Significant correlations were observed between all the VIs (p < 0.05) (Appendix E). Only PSRI had negative correlations with the rest of the IVs.

The functional relationships between forage nutritional parameters and VIs were linear, exponential, and logarithmic. Examples of the developed bidimensional graphs are presented in Fig. 6. The regression models that presented the best fit for each relationship between the forage nutritional parameters and VIs are shown in Table 3 4, 5 and 6. The linear relationship was the most common, found in more than 94% of the relationships evaluated. Despite only three herbage samples being taken to represent the entire plot at each sampling time, all the linear regression models were significant (p < 0.05), and more than 85% presented R^2 greater than 0.5. The VI that showed the best adequacy for estimating the percentage of DM content was NDVI. The functional form that yielded the highest R^2 was the exponential ($R^2 = 0.923$). However, considering that the values of RMSE, rRMSE, and MAE in the linear model are considerably lower than for the exponential model, the linear estimation constitutes the most appropriate model. The values of RMSE in the linear models varied from 12.94 to 24.04% for DM, from 3.48 to 5.25% for CP, from 3.96 to 7.25% for NDF, and from 1.91 to 2.9% for ADF.

4. Discussion

4.1. Weather data

The rainiest months in both available meteorological stations were May, June and July, representing 73% and 60.3% of the annual precipitation in La Estrella and Pumanque, respectively. The weather patterns observed across the two weather stations align with the observed trends of declining precipitation and rising temperatures over the past few decades reported by Garreaud et al. (2020). Chile has been mentioned as susceptible to various effects of climate change, including heat, fires, floods, coastal deterioration, and a projected decrease in precipitation that in 2050 could reach a maximum of 9.3 mm per month (Cortina and Madeira, 2023). This situation can be observed by comparing the average annual precipitation over the last 20 years in the communes of La Estrella (640.2 mm) and Pumanque (477.1 mm) with the 304.2 mm and 319 mm recorded, respectively, in 2018 (CR2, 2025).

4.2. Seasonal variation in forage nutrient content and botanical composition

While on one hand, at least 8% soil moisture (Olivares et al., 1997) or 20 mm of precipitation (Johnston et al., 1998) are required to initiate plant's germination and emergence process; on the other hand, the minimum temperatures for the germination process would be around 4 °C for poaceae and −1 °C for geraniaceae (Olivares et al., 1999). Almost no herbage height increase was observed from June to August but then rose rapidly until November (Fig. 5). Subsequently, a non-significant decrease in the herbage height was observed in December. The senescence process could explain the decrease in herbage height, while the lignification of the herbage could explain the non-significance of this decrease. Moreover, both process are confirmed by the high DM content values observed in the November and December. Concerning nutritional value, the expected trend to increase DM, ADF, and decrease CP as the maturation of the pasture increases was observed after the herbage initiated its seasonal growth (Table 1). October had the lowest DM and ADF concentration and the highest CP concentration than the following months. Riveros et al. (1978) reported that the highest CP content reached in a natural semi-arid prairie was 14% in September, while Squella (1999) indicated a CP range of 12.1 to 4.3% from the vegetative stage (July/August) to seed maturation (November).

Overall, the herbage accumulation observed at the end of the grazing season was low compared to previous values reported for the region (3.5 Ton DM/ha; Castellaro and Squella, 2006), and the herbage nutritional

Table 3
Dry matter (%) prediction models.

Variable	Equation 1	R^2	RMSE (%)	rRMSE	MAE (%)	Equation 2	R^2	RMSE (%)	rRMSE	MAE (%)
GCI	$y = -51.09 \ln(x) + 103.54$	0.835**	13.94	0.540	12.10	$y = 111.81e^{-0.302}$	0.769**	62.18	123.67	54.83
CLRG	$y = -353.18x + 64.47$	0.602**	18.32	0.671	16.13	$y = 55.63e^{-7.169}$	0.388**	63.67	183.42	56.27
GNDVI	$y = -221.04x + 177.78$	0.830**	14.11	0.554	11.84	$y = 659.59e^{-4.762}$	0.830**	62.15	113.34	54.83
NDVI	$y = -91.04x + 80.54$	0.897**	13.49	0.486	11.65	$y = 79.52e^{-1.86}$	0.923**	64.13	128.76	56.69
PSRI	$y = 117.08x + 16.79$	0.823**	12.94	0.441	9.03	$y = 21.78e^{-2.34}$	0.823**	63.44	108.04	55.79
RNDVI	$y = -668.20x + 62.03$	0.665**	18.83	0.929	15.29	$y = 55.03e^{-14.87}$	0.665**	62.21	137.87	54.82
RVI	$y = -32.90 \ln(x) + 84.64$	0.479**	24.04	1.239	20.61	$y = 82.76e^{-0.155}$	0.35**	60.31	222.13	53.22
SAVI	$y = -61.849x + 82.927$	0.759**	15.46	0.563	12.64	$y = 81.98e^{-1.27}$	0.759**	63.49	110.9	55.84

RMSE: Root mean square error (RMSE), MAE: Mean absolute error rRMSE: Relative root mean square error.
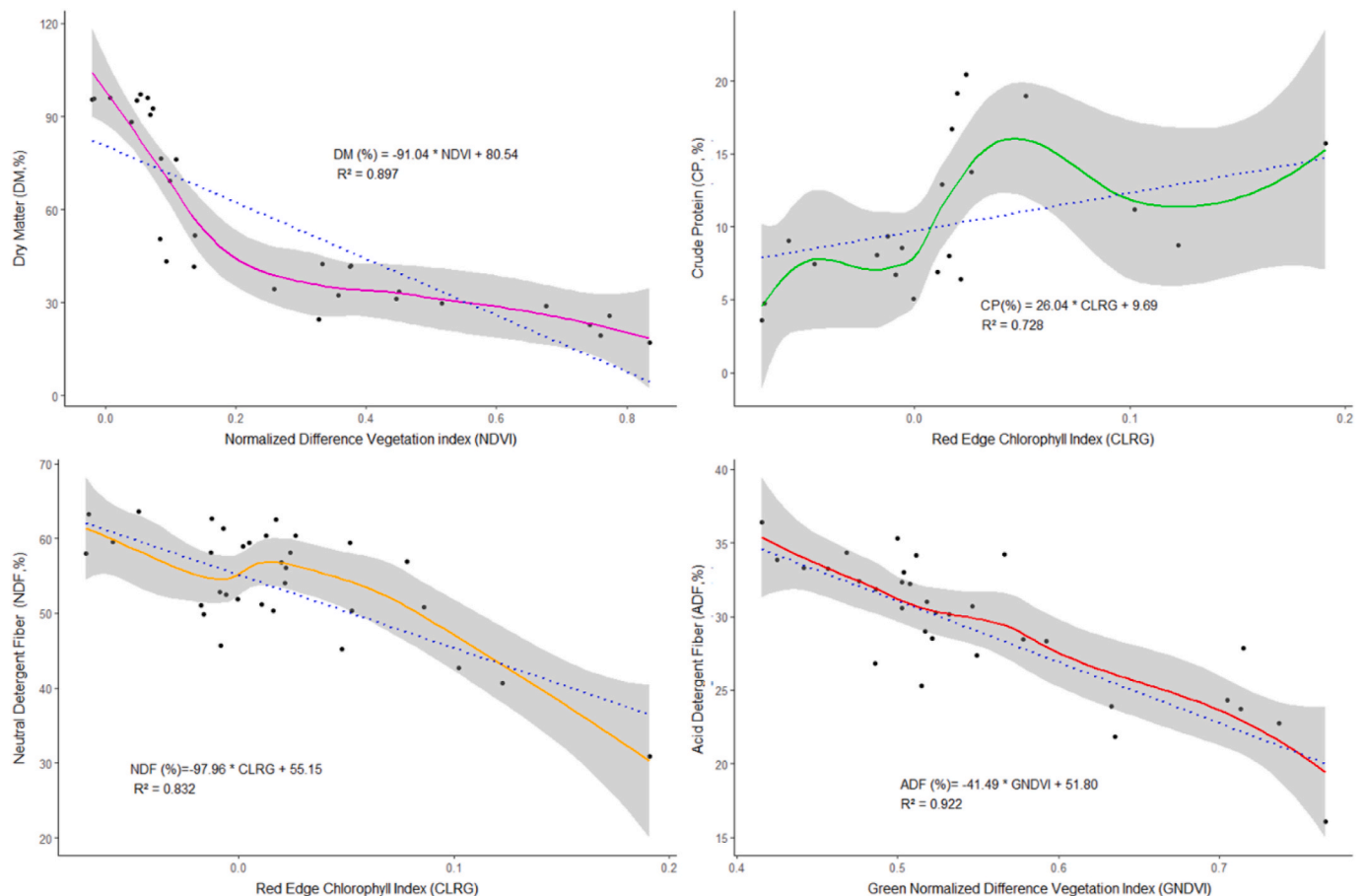
Fig. 6. Functional relationships between forage nutritional parameters (DM, CP, NDF and ADF) and VIs selected (Linear regression model).

value was low, and it is likely that these effects may be related to the mega drought experienced in the region since 2010 (Garreaud et al., 2020; Fuentealba et al., 2021) as observed in Fig. 2. This event has caused two effects on the pastures: a delay in the start of the growing season and a shortened growing period, which has led to a rapid decline in the nutritional value of the forage.

The botanical composition differed among the analyzed sites; this situation is expected when considering the diversity of species in the naturalized grassland; for example, De Miguel et al. (2016), describe more than 40 species present in two sites near the study area. However, the absence of pioneer species such as *Amsinckia hispida, Raphanus sativus,* or *Brassicas* spp., and the presence of *Hordeum murinum*, indicate that the pastures in the analyzed sites were likely in a medium succession stage, ranging from 5 to 10 years (Olivares, 2017).

4.3. Model construction and performance evaluation

The functional forms and trends of the vegetation indices (VIs) were similar to the findings of Almeida-Ñauñay et al. (2022), thus, the NDVI increased during the period of greatest grassland growth and reached minimum values during the senescence stage. As noted by Hill (2013), NDVI represents a wide range of variants sensitive to chlorophyll and photosynthetic vegetation. Therefore, as grass availability and vigor increase, the NDVI value also increases. The positive relationship between NDVI, SAVI, and grass availability has led to their popular use in determining forage biomass in grasslands (Théau et al., 2021; Munyati, 2022). The similarity between NDVI and SAVI is not surprising, as SAVI compensates for the effect of soil in sparsely vegetated areas (Ren et al., 2011; Vani and Mandla, 2017), which is a limitation of NDVI. NDVI, SAVI, and GCI exhibited similar trends during the evaluated months. However, the difference in the values of NDVI and SAVI decreased as the growing season progressed due to the high herbage cover, which

minimized bare soil areas (Table 2). RVI showed little variability in November and December, indicating a similarity in reflectance between NIR and red bands in mature grasses with values close to one. In contrast to RVI, GNDVI uses the green band instead of the red band, making it more sensitive to changes in tonality as the pasture rapidly advances to the senescence stage. Thus, a sharp drop in the value of GNDVI was observed in November, remaining relatively constant in December. RNDVI and CLRG showed similar distributions, with greater variability observed in December compared to the other months for these two VIs (Table 2). The increased variability in December can be attributed to the incorporation of the red edge band in the calculation of these VIs. The red edge band, located between red absorption and NIR reflection, provides greater sensitivity to chlorophyll content and reflects different vitality levels of the pasture (Clevers, 1994).

In this study, all the VIs, except for PSRI, decreased as the growing season progressed. The negative correlation between PSRI and NDVI (Appendix E) aligns with the findings of Hill (2013). The decrease in the value of NDVI as the growing season progressed was described by Di Bella et al. (2004), who associated the senescent cover fraction with NDVI. The increase in PSRI as the growing season progressed was expected, as this VI is based on the chlorophyll/carotenoid ratio, which undergoes significant changes due to the differential breakdown rates of these pigments during early senescence (Anderegg et al., 2020). On the other hand, in GCI, the red band is replaced by the green band, minimizing the importance of color changes to yellow, orange, tan, and brown resulting from pigment breakdown (carotenoids and others) that manifests as chlorophyll breakdown (Proctor et al., 2017). In the study area, chlorophyll breakdown commonly begins in early November, marking the onset of the senescence process, and extends to full pasture senescence in December–January (Ruiz, 1996).

4.4. Model building

Gao et al. (2019) proposed a linear estimation model between RVI (NIR/RED) and herbage DM percentage, while Adrien et al. (2020) used single and multiple linear regression to relate herbage mass with VIs. NDVI and GNDVI have shown high correlations with grassland biomass in previous studies (Jin et al., 2014; Naidoo et al., 2019). The linear relationship between herbage parameters and VIs has been reported by several authors (Jin et al., 2014; Gao et al., 2019; Adrien et al., 2020). Wang et al. (2024) used four vegetation indices (SAVI, RVI, NDVI, and TCI, the Triangular Chlorophyll Index) to define nonlinear prediction models for biomass in the Inner Mongolia Typical Grasslands. The vegetation index that provided the best fit was SAVI, with an R^2 of 0.461 and RMSE values of 104.63. Pan et al. (2024) obtained R^2 values ranging from 0.46 to 0.86, with RMSE values ranging from 109.7 g/m^2 to 226.4 g/m^2 in aboveground biomass (AGB) prediction models. Adrien et al. (2020) reported a mean ($\pm$ standard deviation) dry above-ground biomass of 5494 $\pm$ 929 kg/ha in a Timothy pasture. They obtained maximum R^2 values of 0.54, 0.84, and 0.82 for models estimating CP, NDF, and ADF, respectively. However, the authors did not specify the vegetation indices (VIs) associated with these values. Regarding the prediction of DM, the VI that yielded the best R^2 (0.923) was NDVI when the exponential regression model was used. Nevertheless, lineal regression model exhibited a lower RMSE (13.49%)(Table 3).This was similar to what was observed in CP predicting models, where the RMSE, rRMSE, and MAE values were lower in the linear model. Considering the RMSE values of the linear models and the low CP content of the herbage at the end of the growing season (5.9%), an improvement in the precision of the estimation of this parameter is required. Raab et al. (2020) obtained RMSE values of 1.7% using eight predictor variables selected from a collective of 102 optical-and radar-based predictor variables from the Sentinel-1 and Sentinel-2 satellites to predict herbage CP content. The linear models for NDF and ADF had the best performance, based on the lower RMSE, rRMSE, and MAE and high R^2 values. CLRG had the best fit (R^2 = 0.832) for NDF, while for ADF the most adequate

VI was GNDVI (R^2 = 0.922). Barnetson et al. (2020), who studied the quality of Queensland's rangelands (dry tropical to subtropical) through the use of hyperspectral images, indicated that the visible red (651 nm) and red-edge (759 nm) regions were highly correlated with the CP and ADF concentratios of the pasture. The indicator with the best performance for ADF (GNDVI) considered the NIR and green bands, whereas the selected VI (CLRG) for CP considered the NIR and red-edge bands. In general, the non-linear models showed higher RMSE, rRMSE, and MAE values than the linear models. Since the RMSE value indicates the standard deviation of the unexplained variance in the same unit of measurement of the parameter, the models would not be able to explain much of the error in the estimates of DM and CP. Geipel et al. (2021) developed prediction models of DM, CP, and NDF, among others, for grass-legume mixtures in Southeast and Central Norway, obtaining RMSE of 15.2, 11.7 and 4.8%, respectively, values that do not differ substantially from those obtained in the present study (Tables 3–6).

Secondly, the model with the best MAE (the mean absolute difference between the true value and the predicted value) for DM had a value of 9 for the VI PSRI. The predominance of different species in each study site as consequence of the state of erosion/conservation of the pasture, could be responsible for this phenomenon since, each species had different nutrient concentrations at the same phenological stage. Furthermore, the phenological state varied depending on the soil contents of organic matter, density, moisture retention capacity, and environmental conditions and exposure (Appendix F). Jin et al. (2014) developed specific models for different steppe regions due to the variability of the vegetation present in the grassland types, finding differences in the VIs that provided better predictions according to the study region. Considering these aspects, the use of machine learning algorithm models such as random forest, emerges as an alternative that should be explored (Viljanen et al., 2018). For instance, De Rosa et al. (2021) and Nevavuori et al. (2019) developed statistical models and/or used machine learning algorithms for the prediction of biomass of pastures and crops (wheat and barley). Some of these approaches raise the possibility of using new spectral bands, such as individual bands in red absorption pit to estimate biophysical and biochemical variables in grasslands (Schlerf et al., 2010; Ren and Zhou, 2014).

Although the present study constitutes an advance in using VIs to estimate the quality of pastures in the semi-arid zone of Chile, it has some limitations that must be addressed in future research. The first one is that considering the natural variability of species between and within large farms, the number of samples and sampling sites needs to be larger. One of the reasons for the low number of samples in the study was the cutting protocol given that reaching 3 cm of compressed height delayed the collection of samples until October due to the lower than expected precipitation. Increasing the number of samples and sampling sites would enable the development of more complex models incorporating variables such as seasonality and/or the phenological stage of grasslands. Including these variables is expected to enhance the accuracy of estimates, given the strong correlation between the maturity stage of plants and their nutritional value.

Additionally, although UAV images have high resolution and every day the UAVs increase their flight authonomy time, it is advisable to use images with more coverage and without the need for an operator for large surface areas, such as satellite images. However, satellite images are not free of limitations, including resolution, temporality, band's availability, cost, and the presence of clouds (restricted availability in the winter months) (Fisher et al., 2018; Xu et al., 2018).

In summary, given that both UAV images and satellite images have advantages and disadvantages, a machine learning methodology is required that allows scaling between nutritional quality parameters derived from VIs obtained from UAV multispectral images, with models that relate the information of these images with satellite images of larger coverage, thus allowing the estimation of forage nutritional parameters in larger grasslands areas. Guo et al. (2019) used this approach and developed a drone-based sensing system to collect training data for rice

Table 4
Crude protein (%) prediction models.

Variable	Equation 1	R^2	RMSE (%)	rRMSE	MAE (%)	Equation 2	R^2	RMSE (%)	rRMSE	MAE (%)
GCI	$Y = 0.88x + 7.75$	0.93**	4.91	9.972	3.71	$y = 7.04e^{0.10}$	0.934**	9.67	172.8	8.12
CLRG	$Y = 26.04x + 9.69$	0.728**	4.39	3.217	3.39	$y = 8.82e^{2.79}$	0.728**	9.635	65.78	8.14
GNDVI	$Y = 15.83x + 1.56$	0.875**	4.54	4.581	3.42	$Y = 3.54e^{1.77}$	0.876**	9.645	87.09	8.12
NDVI	$Y = 8.67x + 8.02$	0.448**	4.11	1.394	3.39	$Y = 7.42e^{0.89}$	0.448**	9.807	33.22	8.32
PSRI	$Y = -12.47x + 14.69$	0.598**	3.48	0.869	2.82	$Y = 14.63e^{-1.26}$	0.598**	9.773	24.19	8.34
RNDVI	$Y = 54.82x + 9.75$	0.719**	4.34	2.990	3.37	$Y = 8.88e^{5.91}$	0.719**	9.646	61.59	8.14
RVI	$Y = 0.51x + 9.046$	0.051**	5.25	4.150	4.65	$Y = 2.93\ln(x) + 8.57$	0.193**	4.860	1.86	4.30
SAVI	$Y = 5.78x + 8.02$	0.448**	4.11	1.390	3.39	$Y = 7.42e^{0.59}$	0.448**	9.807	32.22	8.33

Table 5
Neutral detergent fiber (%) prediction models.

Variable	Equation 1	R^2	RMSE (%)	rRMSE	MAE (%)	Equation 2	R^2	RMSE (%)	rRMSE	MAE (%)
GCI	$y = -4.07x + 64.50$	0.765**	4.28	0.623	3.669	$y = 67.27e^{-0.09}$	0.764**	49.84	329.27	49.26
CLRG	$y = -97.96x + 55.15$	0.832**	3.96	0.685	3.709	$y = 54.73e^{-2.14}$	0.832**	49.84	395.34	49.25
GNDVI	$y = -57.66x + 84.76$	0.740**	4.49	0.661	3.78	$y = 103.95e^{-1.25}$	0.740**	49.85	338.97	49.26
NDVI	$y = -18.34x + 58.49$	0.592**	5.22	1.333	6.99	$y = 58.88e^{-0.51}$	0.475**	49.70	336.33	49.13
PSRI	$y = 22.22x + 44.80$	0.431**	7.25	1.396	6.09	$y = 43.64e^{-0.48}$	0.431**	49.68	438.48	49.09
RNDVI	$y = -203.64x + 59.94$	0.826**	4.01	0.703	3.75	$y = 54.48e^{-4.43}$	0.826**	49.84	401.30	49.25
RVI	$y = -1.86x + 58.69$	0.677**	6.52	0.858	5.38	$y = 58.98e^{-0.03}$	0.677**	50.09	314.21	50.09
SAVI	$y = -15.35x + 58.49$	0.475**	8.08	1.204	6.03	$y = 58.88e^{-0.34}$	0.475**	49.71	336.33	49.13

Table 6
Acid detergent fiber (%) prediction models.

Variable	Equation 1	R^2	RMSE (%)	rRMSE	MAE (%)	Equation 2	R^2	RMSE (%)	rRMSE	MAE (%)
GCI	$y = -2.81x + 36.95$	0.886**	1.91	0.434	1.51	$y = -9.59 \ln(x) + 37.89$	0.918**	1.86	0.425	1.39
CLRG	$y = -70.39x + 30.45$	0.303**	3.69	1.062	3.12	$y = 30.17e^{-2.76}$	0.302**	27.39	200.44	27.39
GNDVI	$y = -41.49x + 51.80$	0.922**	1.91	0.439	1.48	$y = 69.04e^{-1.61}$	0.922**	26.87	159.45	26.54
NDVI	$y = -16.81x + 33.50$	0.805**	2.90	0.493	1.97	$y = 33.89e^{-0.64}$	0.805**	26.67	117.19	26.37
PSRI	$y = 18.38x + 22.67$	0.792**	2.39	0.455	1.51	$y = 22.42e^{0.69}$	0.792**	26.65	133.91	26.34
RNDVI	$y = -137.46x + 30.10$	0.895**	2.72	0.862	2.03	$y = 29.75e^{-5.43}$	0.895**	26.89	215.99	26.57
RVI	$y = -1.39x + 33.26$	0.772**	2.90	0.489	2.19	$y = 33.57e^{-0.05}$	0.773**	25.61	112.68	24.97
SAVI	$y = -11.20x + 33.50$	0.805**	2.90	0.493	1.97	$y = 33.89e^{-0.43}$	0.805**	26.67	117.19	26.37

mapping and monitoring in Australia. Given that planning is a critical task in grassland management, it is essential to predict changes in forage availability and quality of grassland over time and in a timely fashion. Thus, in addition to acquiring these variables in real time, it is highly desirable to be able to predict their values in the short and medium term. Under these circumstances, the development of predictive mathematical models based on pasture current information and the climatic variables that determine forage quality is an aspect that deserves to be further studied.

5. Conclusion and implications

The Mediterranean semi-arid rainfed natural grasslands analyzed in this study exhibited a short growing season of only three months, characterized by a typical rise and rapid increase in herbage biomass, DM, ADF, and NDF contents, along with a decline in CP content. Climate factors, such as precipitation and air temperature, have a significant influence on biomass yields and CP content. Therefore, developing more complex and definitive models requires additional years of replication and a more comprehensive treatment of the data. However, the models selected in this study represent initial approximations that highlight the potential for obtaining more accurate estimates of the nutritional quality parameters of naturalized grasslands in Mediterranean semi-arid regions. Under the conditions of this research, the NDVI, CLRG, CLRG, and RNDVI vegetation indices provided the best-fitting linear models for predicting DM, CP, NDF, and ADF, respectively. Developing predictive models based on different VIs, and therefore dependent on different spectral bands, underscores the need to propose new VIs or relationships between more than two bands to better model seasonal changes in grassland quality.

This study highlights the significant potential for linking detailed local data with remote sensing information to model the nutritional value of grasslands over large areas. By integrating VIs derived from multispectral images with field measurements of forage quality, the study provides a scalable and cost-effective approach to assess forage nutritional quality. This is particularly important for sustainable grassland management, as it enables the continuous monitoring of large and heterogeneous areas while reducing the need for labor-intensive and expensive field sampling. The use of UAVs and satellite data offers the flexibility to capture seasonal and spatial variations, which are crucial for understanding and managing the dynamics of grasslands in semi-arid Mediterranean regions. Our findings suggest the importance of integrating various tools, such as precision agriculture technologies and machine learning methods, to support farmers in making informed decisions about the management of extensive grasslands.

CRediT authorship contribution statement

Toro-Mujica P: Writing – review & editing, Writing – original draft, Visualization, Validation, Supervision, Software, Resources, Project administration, Methodology, Investigation, Funding acquisition, Formal analysis, Data curation, Conceptuali. **Lozano-Parra J:** Writing – review & editing, Methodology. **Enríquez-Hidalgo D:** Writing – review & editing, Methodology, In.

Declaration of competing interest

The authors declare that they have no known competing financial

interests or personal relationships that could have appeared to influence the work reported in this paper.

Appendices.

Appendix A
Soil properties of the study areas. OC = Organic carbon (% by weight); BD = Bulk density.

Study Areas	Depth (cm)	% Sand	% Silt	% Clay	OC	BD (kg/dm^3)
S1	0–30	46	21	33	0.66	1.45
	30–100	36	33	31	0.28	1.33
S2	0–30	45	27	28	0.70	1.39
	30–100	41	32	27	0.30	1.36
S3	0–30	51	22	27	0.63	1.45
	30–100	45	21	34	0.35	1.5

Source: Harmonized World Soil Database V1.2

Appendix B. *Exclusion plot and meteorological station*

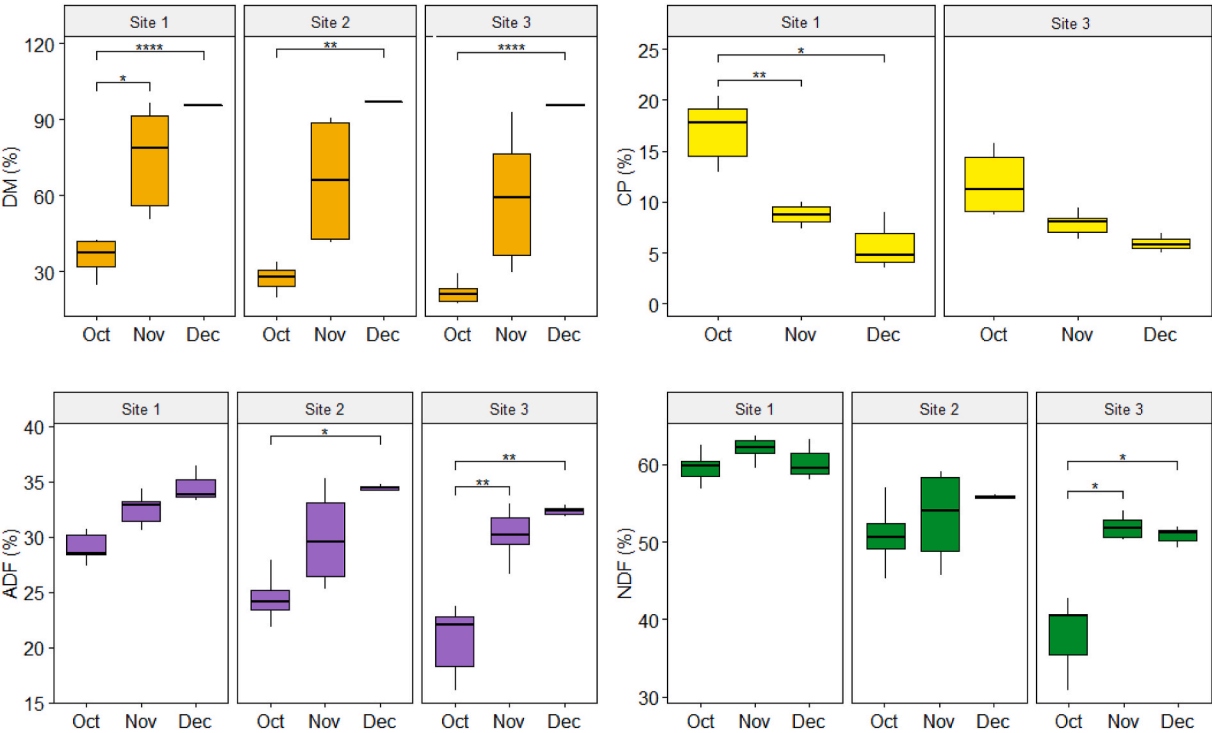### Appendix C
Geographical locations of each exclusor

Sites	Exclusor	Latitude	Length
S1: La Estrella	1	34° 16′34.334″S	71°34′44.098″W
	2	34°16′37.942″S	71°34′44.454″W
	3	34°16′36.106″S	71°34′47.323″W
S2: Marchigüe	1	34°17′35.192″S	71°43′47.352″W
	2	34°17′33.367″S	71°43′44.242″W
	3	34°17′38.656″S	71°43′43.277″W
S3: Pumanque	1	34°32′26.614″S	71°36′40.507″W
	2	34°32′23.716″S	71°36′40.406″W
	3	34°32′22.927″S	71°36′42.775″W

Appendix D

Vegetation Indices Information

Name	Acronyms	Calculation formula	Sources
Ratio Vegetation Index	RVI	$RVI = \dfrac{NIR}{RED}$	Pearson and Miller (1972)
Normalized Difference Vegetation Index	NDVI	$NDVI = \dfrac{NIR - RED}{NIR + RED}$	Rouse et al. (1974)
Green Normalized Difference Vegetation Index	GNDVI	$GNDVI = \dfrac{NIR - GREEN}{NIR + GREEN}$	Gitelson et al. (1996)
Green Chlorophyll Index	GCI	$GCI = \dfrac{NIR}{GREEN} - 1$	Gitelson et al. (2003a)
Red Edge Normalized Difference Vegetation Index	RNDVI	$RNDVI = \dfrac{NIR - RED\ EDGE}{NIR + RED\ EDGE}$	Gitelson and Merzlyak (1994)
Red Edge Chlorophyll Index	CLRG	$CLRG = \left(\dfrac{NIR}{RED\ EDGE}\right) - 1$	Gitelson et al. (2003b)
Soil-Adjusted Vegetation Index	SAVI	$SAVI = \left(\dfrac{NIR - RED}{NIR + RED + L}\right)*(1 + L)$ $L = 0.5$	Huete (1988)
Plant Senescence Reflectance Index	PSRI	$PSRI = \dfrac{RED - GREEN}{NIR}$	Merzlyak et al. (1999)

Appendix E

Correlations between IVs

	GNDVI	NDVI	PSRI	RNDVI	RVI	SAVI	CLG
CLRG	0.9557	0.8991	−0.8311	0.9990	0.8879	0.8991	0.9463
GNDVI		0.9709	−0.9165	0.9539	0.9107	0.9709	0.9766
NDVI			−0.9759	0.8939	0.9087	1.0000	0.9503
PSRI				−0.8291	−0.8121	−0.9759	−0.8658
RNDVI					0.8735	0.8939	0.9371
RVI						0.9087	0.9673
SAVI							0.9503
CLG							

Appendix F. Monthly variation of the composition (DM = Dry Matter, CP = Crude Protein, ADF=Acid Detergent Fiber, NDF = Neutral Detergent Fiber) of the grassland in the study sites (Site 1 = La Estrella, Site 2 = Marchigüe and Site 3 = Pumanque.

Data availability

Data will be made available on request.

References

Adrien, M., Lejeune, P., David, K., Crémer, S., Christian, D., Bindelle, J., 2020. Can low-cost unmanned aerial systems describe the forage quality Heterogeneity? Insight from a Timothy pasture Case study in southern Belgium. Remote Sens. 12, 1650. https://doi.org/10.3390/rs12101650.

Allen, V.G., Batello, C., Berretta, EJ., Hodgson, J., Kothmann, M., Li, X., McIvor, J., Milne, J., Morris, C., Peeters, A., Sanderson, M., 2011. An international terminology for grazing lands and grazing animals. Grass Forage Sci. 66, 2–28. https://doi.org/10.1111/j.1365-2494.2010.00780.x.

Almeida-Ñaunay, A., Benito, B., Quemada, M., Losada, J., Tarquis, A., 2022. Recurrence plots for quantifying the vegetation indices dynamics in a semi-arid grassland. Geoderma 406, 115488. https://doi.org/10.1016/j.geoderma.2021.115488.

Alignier, A., Aviron, S., Farías, a., Arellano, E., Miranda, M., 2021. Landscape context but not management strategies affects the diversity of native and exotic semi-natural vegetation in Mediterranean agroecosystems of Central Chile. Biol. Conserv. 255, 108976. https://doi.org/10.1016/j.biocon.2021.108976.

Anderegg, J., Yu, K., Aasen, H., Walter, A., Liebisch, F., Hund, A., 2020. Spectral vegetation indices to Track senescence dynamics in Diverse wheat Germplasm. Front. Plant Sci. 10 (1749). https://doi.org/10.3389/fpls.2019.01749.

AOAC, 2005. Official Methods of Analysis of AOAC International, eighteenth ed. AOAC International, Gaithersburg.

Asrar, G., Fuchs, M., Kanemasu, E.T., Hatfield, J.L., 1984. Estimating absorbed photosynthetic radiation and leaf area index from spectral reflectance in wheat. Agron. Journal 76, 300–306. https://doi.org/10.2134/agronj1984.00021962007600020029x.

Bannari, A., Morin, D., Bonn, F., Huete, A.R., 1995. A review of vegetation indices. Remote Sens. Rev. 13, 95–120. https://doi.org/10.1080/02757259509532298.

Barnetson, J., Phinn, S., Scarth, P., 2020. Estimating plant pasture biomass and quality from UAV imaging across Queensland's rangelands. AgriEngineering 2, 523–543. https://doi.org/10.3390/agriengineering2040035.

Beeri, O., Phillips, R., Hendrickson, J., Frank, A.B., Kronberg, S., 2007. Estimating forage quantity and quality using aerial hyperspectral imagery for northern mixed-grass prairie. Remote Sensing of Environment 110 (2), 216–225. https://doi.org/10.1016/j.rse.2007.02.027.

Castellaro, G., Squella, F., 2006. A simple simulation model to estimate pasture growth, phenology and water balance of annual pastures of Mediterranean climate. Agric. Tec. (Santiago) 66 (3), 271–282.

Castillo, M., Plaza, Á., Garfias, R., 2020. A recent review of fire behavior and fire effects on native vegetation in Central Chile. Global Ecology and Conservation 24, e01210. https://doi.org/10.1016/j.gecco.2020.e01210.

Clevers, J., 1994. Imaging Spectrometry in Agriculture - Plant Vitality and Yield Indicators, pp. 193–219.

Clevers, J., Gitelson, A., 2013. Remote estimation of crop and grass chlorophyll and nitrogen content using red-edge bands on Sentinel-2 and -3. Int. J. Appl. Earth Obs. Geoinf. 23, 344–351. https://doi.org/10.1016/j.jag.2012.10.008.

CR2, 2025. Center for climate and resilience research. Explorador Climático. https://www.explorador.cr2.cl/.

De Miguel, J., Martín-Forés, I., Acosta-Gallo, B., del Pozo, A., Ovalle, C., Sánchez-Jardón, L., Castro, I., Casado, M., 2016. Non-random co-occurrence of native and exotic plant species in Mediterranean grasslands. Acta Oecol. 77, 18–26. https://doi.org/10.1016/j.actao.2016.08.011.

De Rosa, D., Basso, B., Fasiolo, M., Friedl, J., Fulkerson, B., Grace, P.R., Rowlings, D.W., 2021. Predicting pasture biomass using a statistical model and machine learning algorithm implemented with remotely sensed imagery. Comput. Electron. Agric. 180, 105880. https://doi.org/10.1016/j.compag.2020.105880.

Di Bella, C., Paruelo, J., Becerra, J., Bacour, C., Frederic, B., 2004. Effect of senescent leaves on NDVI-based estimates of fAPAR. Int. J. Rem. Sens. 25, 5415–5427. https://doi.org/10.1080/01431160412331269724.

Dube, T., Shoko, C., Gara, T.W., 2021. Remote sensing of aboveground grass biomass between Remote sensing of aboveground grass biomass between protected and non-protected areas in savannah rangelands. protected and non-protected areas in savannah rangelands. Afr. J. Ecol. 59 (3), 583–796. https://doi.org/10.1111/aje.12856.

Dusseux, P., Guyet, T., Pattier, P., Barbier, V., Nicolas, H., 2022. Monitoring of grassland productivity using Sentinel-2 remote sensing data. Int. J. Appl. Earth Obs. Geoinf. 111. https://doi.org/10.1016/j.jag.2022.102843.

Enriquez-Hidalgo, D., Gilliland, T.J., Hennessy, D., 2016. Herbage and nitrogen yields, fixation and transfer by white clover to companion grasses in grazed swards under different rates of nitrogen fertilization. Grass Forage Sci. 71, 559–574. https://doi.org/10.1111/gfs.12201.

Espinoza, S., Ovalle, C., del Pozo, A., 2020. The contribution of nitrogen fixed by annual legume pastures to the productivity of wheat in two contrasting Mediterranean environments in central Chile. Field Crops Res. 249. https://doi.org/10.1016/j.fcr.2019.107709.

Fajji, N.G., Palamuleni, L.G., Mlambo, V., 2017. Evaluating derived vegetation indices and cover fraction to estimate rangeland aboveground biomass in semi-arid environments. S. Afr. J. Geol. 6 (3), 333–348. https://doi.org/10.4314/sajg.v6i3.5.

FAO, 2012. Harmonized World soil database. FAO/IIASA/ISRIC/ISS-CAS/JRC. V 1.2: Viewer version.

Fenetahun, Y., You, Y., Fentahun, T., Xinwen, X., Yong-Dong, W., 2021 Oct 21. Effects of grazing intensity on forage nutritive value of dominant grass species in Borana rangelands of Southern Ethiopia. PeerJ 9, e12204. https://doi.org/10.7717/peerj.

Fern, R.R., Foxley, E.A., Bruno, A., Morrison, M.L., 2018. Suitability of NDVI and OSAVI as estimators of green biomass and coverage in a semi-arid rangeland. Ecol. Indic. 94, 16–21. https://doi.org/10.1016/j.ecolind.2018.06.02.

Fisher, J.R.B., Acosta, E.A., Dennedy-Frank, P.J., Kroeger, T., Boucher, T.M., 2018. Impact of satellite imagery spatial resolution on land use classification accuracy and modeled water quality. Remote Sensing in Ecology and Conservation 4, 137–149. https://doi.org/10.1002/rse2.61.

Fox, J., Weisberg, S., 2019. An R Companion to Applied Regression, third ed. Sage, Thousand Oaks CA https://socialsciences.mcmaster.ca/jfox/Books/Companion/.

Fox, J., Weisberg, S., Price, B., 2020. carData: companion to Applied regression data Sets. R package version 3.0–4. https://CRAN.R-project.org/package=carData.

Fuentealba, M., Bahamóndez, C., Sarricolea, P., Meseguer-Ruiz, O., Latorre, C., 2021. The 2010–2020 'megadrought' drives reduction in lake surface area in the Andes of central Chile (32° - 36°S). J. Hydrol.: Reg. Stud. 38. https://doi.org/10.1016/j.ejrh.2021.100952.

Gao, R., Kong, Q., Wang, H., Su, Z., 2019. Diagnostic feed values of natural grasslands based on multispectral images acquired by Small unmanned aerial vehicle. Rangel. Ecol. Manag. 72 (6), 916–922. https://doi.org/10.1016/j.rama.2019.06.00.

Garreaud, R.D., Boisier, J.P., Rondanelli, R., Montecinos, A., Sepúlveda, H.H., Veloso-Aguila, D., 2020. The Central Chile Mega Drought (2010–2018): a climate dynamics perspective. Int. J. Climatol. 40 (1), 421–439. https://doi.org/10.1002/joc.6219.

Gitelson, A., Gritz, Y., Merzlyak, M.-N., 2003a. Relationships between leaf chlorophyll content and spectral reflectance and algorithms for non-destructive chlorophyll assessment in higher plant leaves. J. Plant Physiol. 160 (3), 271–282. https://doi.org/10.1078/0176-1617-00887.

Gitelson, A., Viña, A., Arkebauer, T., Rundquist, D., Keydan, G., Leavitt, B., 2003b. Remote estimation of leaf area index and green leaf biomass in maize canopies. Geophys. Res. Lett. 30 (5), 1248. https://10.1029/2002GL016450.

Gitelson, A.A., Kaufman, Y.J., Merzlyak, M.N., 1996. Use of a green channel in remote sensing of global vegetation from EOS-MODIS. Remote Sensing of Environment 58, 289–298. https://doi.org/10.1016/S0034-4257(96)00072-7.

Gitelson, A.A., Vina, A., Ciganda, V., Rundquist, D.C., Arkebauer, T.J., 2005. Remote estimation of canopy chlorophyll content in crops. Geophys. Res. Lett. 32 (8), L08403. https://doi.org/10.1029/2005GL022688.

Gitelson, A.A., Merzlyak, M.N., 1994. Spectral reflectance changes associated with autumn senescence of Aesculushippocatanum I and Hacer plantanoides I. leaves. Spectral features and relation to chlorophyll estimation. J. Plant Physiol. 143, 286–292. https://doi.org/10.1016/S0176-1617(11)81633-0, 1994.

Geipel, J., Bakken, A.K., Jorgensen, M., Korsaeth, A., 2021. Forage yield and quality estimation by means of UAV and hyperspectral imaging. Precis. Agric. 22 (7). https://doi.org/10.1007/s11119-021-09790-2.

Guo, Y., Jia, X., Paull, D., Zhang, J., Farooq, A., Chen, X., 2019. A drone-based sensing system to support satellite image analysis for rice farm mapping. IGARSS 2019 - 2019 IEEE International Geoscience and Remote Sensing Symposium, pp. 9376–9379. https://doi.org/10.1109/IGARSS.2019.8898638. Yokohama, Japan, 2019.

Harris, I., Osborn, T.J., Jones, P., Lister, D., 2020. Version 4 of the CRU TS monthly high-resolution gridded multivariate climate dataset. Sci. Data 7, 109. https://doi.org/10.1038/s41597-020-0453-3.

Hill, M.J., 2013. Vegetation index suites as indicators of vegetation state in grassland and savanna: an analysis with simulated SENTINEL 2 data for a North American transect. Remote Sensing of Environment 137, 94–111. https://doi.org/10.1016/j.rse.2013.06.004.

Huete, A.R., 1988. A soil-adjusted vegetation index (SAVI). Remote Sensing of Environment 25, 295–309. https://doi.org/10.1016/0034-4257(88)90106-X.

Jin, Y., Yang, X., Qiu, J., Li, J., Gao, T., Wu, Q., Zhao, F., Ma, H., Yu, H., Xu, B., 2014. Remote sensing-based biomass estimation and its Spatio-temporal variations in temperate grassland, northern China. Remote Sens. 6 (2), 1496–1513. https://doi.org/10.3390/rs6021496.

Johnston, M., Olivares, A., y Contreras, X., 1998. El banco de semillas del suelo en respuesta a regímenes pluviométricos simulados. II Géneros de interés forrajero. Av. Prod. Anim. 23 (1–2), 55–65.

Kuhn, M., 2021. Caret: classification and regression training. R package version 6, 0-88. https://CRAN.R-project.org/package=caret.

Liu, Y., Zhang, Z., Tong, L., Khalifa, M., Wang, Q., Gang, C., Wang, Z., Li, J., Sun, Z., 2019. Assessing the effects of climate variation and human activities on grassland degradation and restoration across the globe. Ecol. Indic. 106. https://doi.org/10.1016/j.ecolind.2019.105504.

Lussem, U., Bolten, A., Gnyp, M.L., Jasper, J., Bareth, G., 2018. Evaluation of RGB-based vegetation indices from UAV imagery to estimate forage yield in grassland. Int. Arch. Photogram. Rem. Sens. Spatial Inf. Sci. XLII-3, 1215–1219. https://doi.org/10.5194/isprs-archives-XLII-3-1215-2018.

Lussem, U., Bolten, A., Menne, J., Gnyp, M.L., Schellberg, J., Bareth, G., 2019. Estimating biomass in temperate grassland with high resolution canopy surface models from UAV-based RGB images and vegetation indices. J. Appl. Remote Sens. 13 (3), 034525. https://doi.org/10.1117/1.JRS.13.034525.

Mangewa, L.J., Ndakidemi, P.A., Alward, R.D., Kija, H.K., Bukombe, J.K., Nasolwa, E.R., Munishi, L.K., 2022. Comparative assessment of UAV and Sentinel-2 NDVI and GNDVI for Preliminary Diagnosis of Habitat conditions in Burunge Wildlife management area, Tanzania. Earth 3, 769–787. https://doi.org/10.3390/earth3030044.

Merzlyak, M.N., Gitelson, A.A., Chivkunova, O.B., Rakitin, V.Y., 1999. Non-destructive optical detection of pigment changes during leaf senescence and Fruit Ripening. Physiol. Plantarum 106, 135–141. https://doi.org/10.1034/j.1399-3054.1999.106119.x.

Molle, G., Decandia, M., Cabiddu, A., Landau, SY., Cannas, A., 2008. An update on the nutrition of dairy sheep grazing Mediterranean pastures. Small Rumin. Res. 77 (2–3), 93–112. https://doi.org/10.1016/j.smallrumres.2008.03.003.

Munyati, C., 2022. Detecting the distribution of grass aboveground biomass on a rangeland using Sentinel-2 MSI vegetation indices. Adv. Space Res. 69 (2), 1130–1145. https://doi.org/10.1016/j.asr.2021.10.048.

Naidoo, L., van Deventer, H., Ramoelo, A., Mathieu, R., Nondlazi, B., Gangat, R., 2019. Estimating above ground biomass as an indicator of carbon storage in vegetated wetlands of the grassland biome of South Africa. Int. J. Appl. Earth Obs. Geoinf. 78, 118–129. https://doi.org/10.1016/j.jag.2019.01.021.

Nevavuori, P., Narra, N., Lipping, T., 2019. Crop yield prediction with deep convolutional neural networks. Comput. Electron. Agric. 163. https://doi.org/10.1016/j.compag.2019.104859.

Olivares, A., 2017. La pradera anual de clima mediterráneo (Capitulo III). In: El espinal, manejo silvopastoril de un recurso ignorado.1ª edición. Santiago de Chile, Pag, pp. 35–91.

Olivares, A., Johnston, M., andBeck, C., 1997. Emergencia de especies de pradera natural de tipo mediterráneo en relación con la humedad del suelo. Av. Prod. Anim. 22 (1–2), 23–29.

Olivares, A., Johnston, M., Ramírez, R., 1999. Umbrales de temperatura y humedad en la germinación de tres especies de la pradera anual de clima mediterráneo. Agrociencia 15 (1), 19–26.

Oliveira, R., Näsi, R., Niemeläinen, O., Nyholm, L., Alhonoja, K., Kaivosoja, J., Jauhiainen, L., Viljanen, K., Nezami, S., Markelin, L., Hakala, T., Honkavaara, E., 2020. Machine learning estimators for the quantity and quality of grass swards used for silage production using drone-based imaging spectrometry and photogrammetry. Remote Sensing of Environment 246. https://doi.org/10.1016/j.rse.2020.111830.

Paltsyn, M.Y., Gibbs, J.P., Iegorova, L.V., Mountrakis, G., 2017. Estimation and prediction of grassland cover in Western Mongolia using MODIS-derived vegetation indices. Rangel. Ecol. Manag. 70 (6), 723–729. https://doi.org/10.1016/j.rama.2017.05.005.

Pan, T., Ye, H., Zhang, X., Liao, X., Wang, D., Bayin, D., Safarov, M., Okhonniyozov, M., Majid, G., 2024. Estimating aboveground biomass of grassland in central Asia mountainous areas using unmanned aerial vehicle vegetation indices and image textures – A case study of typical grassland in Tajikistan. Environ. Sustain. Indic. 22. https://doi.org/10.1016/j.indic.2024.100345.

Park, R.S., Agnew, R.E., Gordon, F.J., Steen, R.W.J., 1998. The use of near infrared reflectance spectroscopy (NIRS) on undried samples of grass silage to predict chemical composition and digestibility parameters. Anim. Feed Sci. Technol. 72 (1), 155–167. https://doi.org/10.1016/S0377-8401(97)00175-2.

Pearson, R.L., Miller, L.D., 1972. Remote mapping of standing crop biomass for estimation of the productivity of the shortgrass prairie, Pawnee National Grasslands, Colorado. Proceedings of the 8th International Symposium on Remote Sensing of the Environment II, 1355–1379.

Picard, R.R., Berk, K.N., 1990. Data Splitting. Am. Statistician 44 (2), 140–147.

Pizarro, J., 2007. Atlas climatológico de Chile. In: Torres, G. (Ed.), Campos térmicos y pluviométricos, Dirección General de Aeronautica Civil, Dirección Metereológica de Chile, p. 152. Santiago, Chile (2007).

Poley, L., McDermid, G., 2020. A Systematic review of the factors influencing the estimation of vegetation aboveground biomass using unmanned aerial systems. Remote Sens. 12 (7), 1052. https://doi.org/10.3390/rs12071052.

Posada-Asprilla, W., Medina-Sierra, M., Cerón-Muñoz, M., 2019. Estimación de la calidad y cantidad de pasto kikuyo (Cenchrus clandestinum (Hochst. ex Chiov.) Morrone) usando imágenes multiespectrales. Revista U.D.C.A Actualidad & Divulgación Científica 22 (1), 1–10. https://doi.org/10.31910/rudca.v22.n1.2019.1195.

Proctor, C., Lu, B., He, Y., 2017. Determining the absorption coefficients of decay pigments in decomposing monocots. Remote Sensing of Environment 199, 137–153. https://doi.org/10.1016/j.rse.2017.07.007.

R Core Team, 2021. R: A Language and Environment for Statistical Computing. R Foundation for Statistical Computing, Vienna, Austria. https://www.R-project.org/.

Raab, C., Riesch, F., Tonn, B., Barrett, B., Meißner, M., Balkenhol, N., Isselstein, J., 2020. Target-oriented habitat and wildlife management: estimating forage quantity and quality of semi-natural grasslands with Sentinel-1 and Sentinel-2 data: Grassland Quantity and Quality Using Satellites. Remote Sensing Ecol. Conserv. 6. https://doi.org/10.1002/rse2.149.

Ramoelo, A., Skidmore, A.K., Cho, M.A., Schlerf, M., Mathieu, R., Heitkönig, I.M.A., 2012. Regional estimation of savanna grass nitrogen using the red-edge band of the spaceborne RapidEye sensor. Int. J. Appl. Earth Obs. Geoinf. 19, 151–162. https://doi.org/10.1016/j.jag.2012.05.009.

Ren, H., Zhou, G., 2014. Estimating aboveground green biomass in desert steppe using band depth indices. Biosyst. Eng. 127, 67–78. https://doi.org/10.1016/j.biosystemseng.2014.08.014.

Ren, H., Zhou, G., Zhang, X., 2011. Estimation of green aboveground biomass of desert steppe in Inner Mongolia based on red-edge reflectance curve area method. Biosyst. Eng. 109 (4), 385–395. https://doi.org/10.1016/j.biosystemseng.2011.05.004.

Riveros, E., Neuman, E., Olivares, A., Manterola, H., Ramírez, R., 1978. Variaciones estacionales en el contenido de caroteno y proteína de la pradera natural y del forraje consumido por ovinos en ecosistemas semiáridos. Av. Prod. Anim. 3, 23–30.

Rouse, J.W., Haas, R.W., Schell, J.A., Deering, D.W., Harlan, J.C., 1974. Monitoring the Vernal Advancement and Retrogradation (Greenwave Effect) of Natural Vegetatioa NASA/GSFCT Type III Final Report. Greenbelt, MD, USA.

Ruiz, N., 1996. Praderas para Chile. Instituto de investigación Agropecuarias (INIA), 2ª ed, p. 733. Santiago, Chile.

Savory Institute, 2018. Ecological outcome verification (EOV). URL:, Version 1.0. https://savory.global/wp-content/uploads/2018/08/0828_EOVDoc.pdf.

Schlerf, M., Atzberger, C., Hill, J., Buddenbaum, H., Werner, W., Schüler, G., 2010. Retrieval of chlorophyll and nitrogen in Norway spruce (Picea abies L. Karst.) using imaging spectroscopy. Int. J. Appl. Earth Obs. Geoinf. 12 (1), 17–26. https://doi.org/10.1016/j.jag.2009.08.006.

Serrano, J., Shahidian, S., Silva, J., 2016. Calibration of GrassMaster II to estimate green and dry matter yield in Mediterranean pastures: effect of pasture moisture content. Crop Pasture Sci. 67 (7), 780–791. https://doi.org/10.1071/CP15319.

Squella, F., 1999. Validación de recursos forrajeros y uso de prácticas de manejo del pastizal natural Informe Técnico, 1998. FIA (PRODECOP-SECANO) - INIA, Centro Regional de Investigación La Platina, p. 56. Santiago, Chile.

Tang, S., Wang, K., Xiang, Y., Tian, D., Wang, J., Liu, Y., Cao, B., Guo, D., Niu, S., 2019. Heavy grazing reduces grassland soil greenhouse gas fluxes: a global meta-analysis. Sci. Total Environ. 654, 1218–1224. https://doi.org/10.1016/j.scitotenv.2018.11.082.

Toro-Mujica, P., García, A., 2025. Effect of forage alternatives on the carbon footprint, productivity, and profitability of sheep production systems in dryland Mediterranean zone of Chile: a simulation model. Ecol. Model. 500. https://doi.org/10.1016/j.ecolmodel.2024.110958.

Théau, J., Lauzier-Hudon, É., Aubé, L., Devillers, N., 2021. Estimation of forage biomass and vegetation cover in grasslands using UAV imagery. PLoS One 16, e0245784. https://doi.org/10.1371/journal.pone.0245784.

Thomson, A.L., Humphries, D.J., Rymer, C., Archer, J.E., Grant, N.W., Reynolds, C.K., 2018. Assessing the accuracy of current near infra-red reflectance spectroscopy analysis for fresh grass-clover mixture silages and development of new equations for this purpose. Anim. Feed Sci. Technol. 239, 94–106. https://doi.org/10.1016/j.anifeedsci.2018.03.009.

Van Soest, P.J., Robertson, J.B., Lewis, B.A., 1991. Methods for dietary fiber, neutral detergent fiber, and Nonstarch Polysaccharides in relation to Animal nutrition. J. Dairy Sci. 74 (10), 3583–3597. https://doi.org/10.3168/jds.S0022-0302(91)78551-2.

Vani, V., Mandla, V., 2017. Comparative study of NDVI and SAVI vegetation indices in Anantapur district semi-arid areas. Int. J. Civ. Eng. Technol. 8, 559–566.

Viljanen, N., Honkavaara, E., Nasi, R., Hakala, T., Niemelainen, O., Kaivosoja, J., 2018. A novel machine learning method for estimating biomass of grass swards using a Photogrammetric canopy height model, images and vegetation indices captured by a drone. Agriculture-Basel 8. https://doi.org/10.3390/agriculture8050070.

Villoslada Peciña, M., Bergamo, T.F., Ward, R.D., Joyce, C.B., Sepp, K., 2021. A novel UAV-based approach for biomass prediction and grassland structure assessment in coastal meadows. Ecol. Indic. 122. https://doi.org/10.1016/j.ecolind.2020.107227.

Wachendorf, M., Fricke, T., Möckel, T., 2018. Remote sensing as a tool to assess botanical composition, structure, quantity and quality of temperate grasslands. Grass Forage Sci. 73 (1), 1–14. https://doi.org/10.1111/gfs.12312.

Wang, R., Dong, J., Jin, L., Sun, Y., Baoyin, T., Wang, X., 2024. Improving the accuracy of vegetation index Retrieval for biomass by combining ground-UAV hyperspectral data–A new method for Inner Mongolia typical grasslands. Phyton-International Journal of Experimental Botany 93 (2), 387–411. https://doi.org/10.32604/phyton.2024.047573.

Wickham, H., Averick, M., Bryan, J., Chang, W., McGowan, L.D., François, R., Grolemund, G., Hayes, A., Henry, L., Hester, J., Kuhn, M., Pedersen, T.L., Miller, E., Bache, S.M., Müller, K., Ooms, J., Robinson, D., Seidel, D.P., Spinu, V., Takahashi, K., Vaughan, D., Wilke, C., Woo, K., Yutani, H., 2019. Welcome to the tidyverse. J. Open Source Softw. 4 (43). https://doi.org/10.21105/joss.01686.

Xu, C., Jae, Lim, J., Jin, X., Yun, H., 2018. Land cover mapping and availability evaluation based on drone images with Multi-spectral camera. Journal of the Korean Society of Surveying, Geodesy, Photogrammetry and Cartography 36 (6), 589–599. https://doi.org/10.35762/AER.2021.43.4.4.

Xu, D., Wang, C., Chen, J., Shen, M., Shen, B., Yan, R., Li, Z., Karnieli, A., Chen, J., Yan, Y., Wang, X., Chen, B., Yin, D., Xin, X., 2021. The superiority of the normalized difference phenology index (NDPI) for estimating grassland aboveground fresh biomass. Remote Sensing of Environment 264. https://doi.org/10.1016/j.rse.2021.112578.

Zhou, X., Huang, W., Zhang, J., Kong, W., Casa, R., Huang, Y., 2019. A novel combined spectral index for estimating the ratio of carotenoid to chlorophyll content to monitor crop physiological and phenological status. Int. J. Appl. Earth Obs. Geoinf. 76, 128–142. https://doi.org/10.1016/j.jag.2018.10.012.